Journal of Power Sources, 3 (1978) 1 - 22

THE DEVELOPMENT OF BETA-ALUMINA FOR USE IN ELECTROCHEMICAL CELLS: A SURVEY*

G. J. MAY

Chloride Silent Power Limited, Davy Road, Astmoor, Runcorn, Cheshire WA7 1PZ (Gt. Britain)

(Received October 10, 1977; in revised form February 9, 1978)

Summary

The use of beta-alumina as a solid ionic conductor in a variety of power sources is now well established. The properties of beta-alumina with regard to these devices are discussed with particular reference to the sodium–sulphur battery. The relationships between phase composition and microstructure with ionic conductivity and mechanical strength are considered and the constraints these properties place on cell design are outlined. Recent experimental data on the mechanical and electrical behaviour of beta-alumina are reported and critical problems for the successful application of beta-alumina are identified.

Introduction

The development of electrochemical power sources with high energy and power densities has stimulated research work on the properties and methods of manufacture of beta-alumina in a large number of laboratories [1, 2]. Much of this work is directed towards the development of the sodium–sulphur battery for motive power and load levelling applications although its use in other power sources is also being considered. Beta-alumina functions as the electrolyte and separator in these devices because it is permeable to sodium ions and is essentially impermeable to electronic charge carriers. In this paper, the requirements for beta-alumina electrolyte materials in various power sources are considered. The ceramic manufacturing processes used and the relationship between these routes and the mechanical and electrical properties of beta-alumina are described. Other properties important to the successful operation of electrochemical cells are outlined, including thermal

*Paper presented at The International Symposium on Molten Electrolytes and High Temperature Batteries organized by the Electrochemistry Group of the Chemical Society, Brighton, Gt. Britain, September 22 - 23, 1977.

shock resistance, wetting of beta-alumina by liquid sodium and its resistance to stress corrosion cracking in liquid sodium.

The high ionic conductivity of beta-alumina results from its crystal structure which consists of layers in which sodium ions are relatively mobile separated by non-conductive layers of aluminium and oxygen ions. In detail, the structure is comprised of four close-packed layers of oxygen ions with aluminium ions in the interstices in the same positions as in the $MgAl_2O_4$ spinel structure if the difference between the magnesium and aluminium ions is ignored (Fig. 1). These layers, referred to as spinel blocks, are bonded

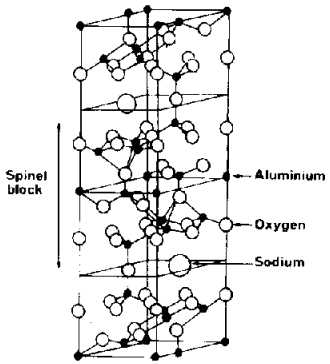

Fig. 1. Crystal structure of beta-alumina.

together by Al–O–Al bonds and sodium ions which are free to move in this plane in an electric field. There are two principal forms of beta-alumina; β- (hexagonal; $P6_3/mmc$; a_0 = 0.559 nm, c_0 = 2.261 nm) [3, 4] and β''- (rhombohedral; $R\bar{3}m$; a_0 = 0.560 nm, c_0 = 3.395 nm [5, 6]. These differ in the stacking sequence of the spinel blocks in that the β- or 2-block structure has a two-fold screw axis and the β''- or 3-block structure has a three-fold screw axis. β''-alumina tends to be more conductive than β- and is stabilized by small doping additions of lithium and magnesium that substitute for aluminium in the spinel blocks. The conduction plane is also an easy cleavage plane because of the relative weakness of bonding across this plane and in practical electrochemical devices mechanical strength is required, as well as high ionic conductivity, to permit the use of thin membranes giving low overall cell impedances. Mechanical strength is achieved by the use of fine-grained polycrystalline materials and also by the elimination of microstructural defects. Large, thin-walled tubes can be readily produced by a variety of ceramic routes and have been successfully utilized in a number of devices.

The sodium–sulphur cell [7 - 12] utilizes beta-alumina as the electrolyte with sodium and sulphur as the two electrodes (Fig. 2). The sulphur electrode contains a matrix of graphite felt which serves as an electron injector and on discharge, sodium ions travel through the electrolyte to form sodium polysulphides over a range of stoichiometry. Cells are operated between 595 and 625 K to keep the discharge products in the liquid state and

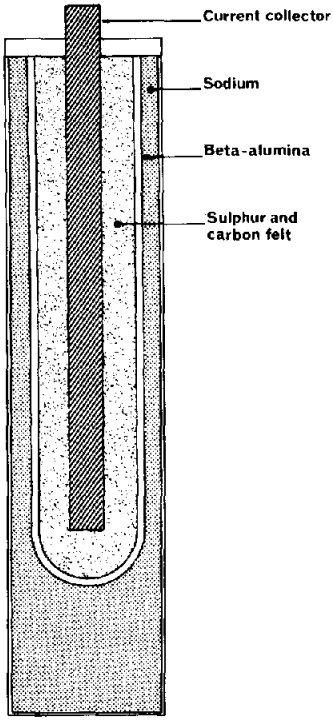

Fig. 2. Schematic diagram of sodium–sulphur cell.

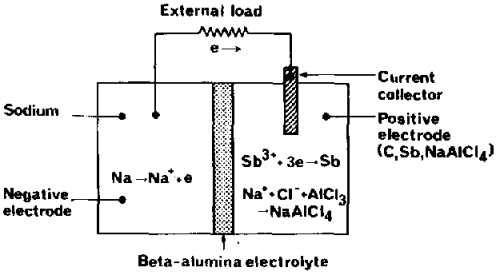

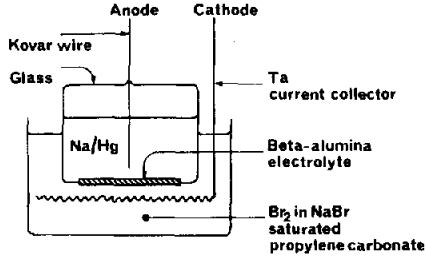

Fig. 3. Schematic representation of sodium/beta-alumina/antimony chloride–sodium chloroaluminate cell.

Fig. 4. Schematic diagram of sodium/mercury amalgam–bromine cell.

although this increases the conductivity of the beta-alumina electrolyte it also defines very stringent materials requirements for the current collector and the seal.

An alternative to the sodium–sulphur cell is the sodium–chloride system [13] which also uses a beta-alumina electrolyte but operates at ~ 475 K permitting the use of polymeric seals and metallic current collectors in the antimony chloride/sodium chloroaluminate cathode (Fig. 3). The lower operating temperature reduces the conductivity of the electrolyte making it

difficult to obtain low overall cell impedances. Beta-alumina has been used in high energy density primary batteries with sodium–mercury amalgam as the anode and halogens, water, or air as the oxidants [14] (Fig. 4). For sodium amalgam/bromine cells, open circuit voltages of 3.8 V and operating voltages of 3.5 V at 1 A/m^2 have been obtained at room temperature. Cells have been described with a stored energy corresponding to 350 Wh/kg and operated for 4 years. The self-discharge rate is negligible but cells do not perform at high power levels or at temperatures much below 300 K. All solid-state cells utilizing a beta-alumina electrolyte separating alkali ferrite electrodes which act as mixed ionic/electronic conductors have also been studied [15, 16] but do not appear to be useful as power sources (Fig. 5).

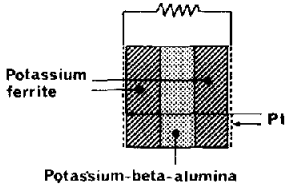

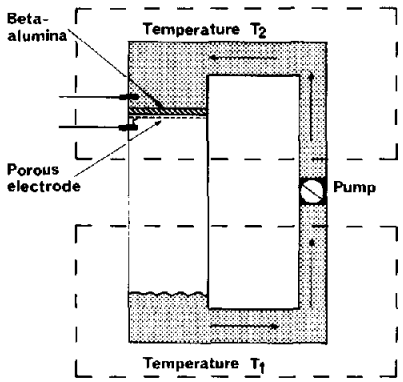

Fig. 5. Schematic diagram of all solid state cell with potassium ferrite electrodes and potassium–beta-alumina electrolyte. Potassium ferrite exists over a range of stoichiometry and the potassium is, in general, at different activities in the two electrodes.

Fig. 6. Schematic diagram of thermoelectric generator using a beta-alumina membrane.

Beta-alumina may be used in an elegant thermoelectric device that converts heat directly to electrical energy [17] (Fig. 6). The thermoelectric generator uses sodium as a working fluid and two regions are separated by a beta-alumina membrane. Liquid sodium at an elevated pressure and temperature migrates through the membrane in the form of sodium ions to a lower pressure region under the driving force of the pressure differential. Electrons flow round an external circuit from one side of the membrane to the other. Sodium metal evaporates from the low pressure side of the membrane and is condensed in a low temperature region. Liquid sodium is then pumped electromagnetically or by means of a wick to the high pressure region, thus completing the cycle. The work done is equivalent to the isothermal expansion of sodium and since no mechanical parts move, the work output is electrical only. Under ideal no load conditions the thermodynamic efficiency approaches the Carnot limit and power outputs of 5 kW/m^2 appear feasible. The main question regarding this application is the long term durability of beta-alumina at operating temperatures which would be typically 1075 K

but since sodium is being evaporated from the ion neutralization surface some of the proposed degradation mechanisms may be inoperative.

Beta-alumina may also find application as an ion selective membrane in a variety of chemical manufacturing processes and in measuring devices. As an example of the former, electrolysis of sodium chloride using a beta-alumina membrane produces chlorine, sodium hydroxide and hydrogen of high purity and with high electrical efficiency but again, the durability of the membrane is likely to be the limiting factor [18]. An example of the latter application is the determination of sodium contents of liquid aluminium and aluminium alloys using a beta-alumina probe [19]. In this device, beta-alumina is used as a reference electrode and as the electrolyte. Voltages proportional to the sodium concentration are produced and immediate analysis is possible.

For application in a power source, a beta-alumina membrane needs to have a low impedance per unit area in order to achieve high power densities, and long-term durability under operating conditions. Low impedance can be obtained either by having a thin membrane or with a material having a high conductivity. The overall impedance of a cell can also be reduced by extending the area of the electrodes and electrolyte and reducing their thickness. These requirements define the physical shape and the material properties of the beta-alumina electrolyte. The various ways in which these are achieved are discussed below.

Ceramic manufacturing processes

The commercial realization of the sodium–sulphur battery and other power sources utilizing beta-alumina as the electrolyte has been impeded by a number of materials problems, not the least of which is the electrolyte itself. This is because the manufacturing problems of beta-alumina have proved to be much more severe than for comparable ceramic materials and also because the performance and durability of the ceramic in cells is sensitive to its microstructure and composition. These problems are largely defined by the volatility of sodium oxide at elevated temperatures which precludes conventional sintering techniques above 1675 K. In common with other ceramic materials beta-alumina is manufactured by sintering a consolidated powder in the solid state and so it is convenient to separate the manufacturing processes into the three stages of powder preparation, green body formation and sintering techniques.

Powder preparation

Powder preparation techniques may be separated arbitrarily into those in which a mixture of materials react together to form beta-alumina subsequent to the green forming stage and those in which beta-alumina is formed before the powder is consolidated. All routes seek to produce materials with a high degree of homogeneity, sintering activity and, when isostatic pressing

is used to produce green shapes, the flow properties of the powder become important.

Most workers have used beta-alumina or alpha-alumina powders together with various additions to produce the desired phase composition. Chemical methods of preparing beta-alumina have been investigated, and also, direct synthesis by fusion. This latter technique has been used to prepare magnesia- and zirconia-doped compositions [17]. Sodium carbonate and α-alumina were induction melted together in a water-cooled copper crucible to form beta-alumina with small additions of magnesia and zirconia. The fused mass was then crushed, milled in a stainless-steel ball mill and metallic impurities were leached out of the powder with hydrochloric acid. The powder was homogeneous, free from metallic impurities and had satisfactory sintering activity.

A number of chemical methods have been investigated, *e.g.*, melt decomposition of mixed nitrates [20], spray decomposition of nitrates [20], decomposition of oxalates or alkoxides [20, 21] or decomposition of organic gels [22]. All of these processes produce powders with an exceptionally high degree of homogeneity because they mix the constituents in the liquid phase. Spray decomposition of mixed solutions of sodium, magnesium and aluminium nitrate produces partly decomposed powders with satisfactory flow properties but further calcining and milling are needed to improve the density and microstructural control of the ceramic [20]. Gel processing has been used to prepare homogeneous beta-alumina powders [22, 25]. In this process, an ethylene glycol–water solution of sodium, lithium and aluminium citrates with excess citric acid is heated to evaporate excess solvent and form a rigid transparent polyester gel which is then heated and decomposed to a fine, homogeneous powder. The powder has a very high specific surface area and produces good quality ceramic.

Beta-alumina powders can be produced by direct mixing of α-alumina or β-alumina powders with Na_2O added as Na_2CO_3, $NaNO_3$, NaOH or $NaAlO_2$, MgO as $Mg(NO_3)_2$ or MgO itself and Li_2O as Li_2CO_3, LiOH or ξ-alumina ($Li_2O.5Al_2O_3$). These materials may be dry milled together in vibratory mills or wet milled in various organic solvents. The use of ξ-alumina is an effective way of dispersing a small quantity of the doping addition in a large volume of powder [26]. Spray drying is being examined as a means of preparing homogeneous free-flowing powders in a number of laboratories [19, 24]. Spray drying with all components in aqueous solution has been investigated and also an all slurry route where a preconverted beta-alumina powder is spray dried as well as a slurry/solution route with α-alumina in suspension and the Na_2O, Li_2O or MgO in solution as Na_2CO_3 and the respective nitrates. Organic dispersants may be used to increase the solids content and stability of the slurry.

Green body formation

Isostatic pressing is a simple technique in which powders contained in a shaped rubber bag with a steel mandrel are compacted by applying a

hydraulic pressure (150 - 400 MN/m^2) to the outside of the bag [24, 27]. The powder is compacted isostatically to a high density and good dimensional tolerances are achieved. Closed-ended tubes with thin walls and lengths of over 500 mm can be fabricated and for wall thicknesses less than 1 mm the green shapes can be machined. The principal requirement for isostatic pressing in large quantities is a free flowing powder that will fill the mould cavity with a reproducible quantity of powder which can be achieved with spray dried or freeze-dried powders.

Electrophoretic deposition uses an electrically charged mandrel placed in a suitable dielectric liquid with a suspension of β-alumina [17, 28 - 30]. An electric field is applied between the mandrel and a suitable counter electrode and powder is deposited uniformly onto the mandrel to build a thickness of ~ 1 mm in a few minutes. Removal from the mandrel is sometimes difficult and involves extended drying periods. Additives in the powder such as aluminium stearate and a high surface finish on the mandrel facilitate removal. Isostatic pressing has been used to improve the homogeneity of the green density and make removal from the mandrel easier by inducing a small amount of springback in the compact.

Extrusion is potentially a very cheap method of making large quantities of open-ended beta-alumina tubing, but there are problems in the development of a suitable binder system to permit rapid extrusion with moderate forces. Binder systems consisting of poly(vinyl pyrrolidone) and ethylene glycol with small additions of colloidal fibrillar hydrated alumina and of hot beeswax have both been shown to be effective although extrusion forces were high and sintered densities were moderate [23]. Other processes such as slip casting [31] and centrifugal casting have also been investigated.

Sintering techniques

There are three main problems in the sintering of beta-alumina some of which are peculiar to this material. These are: (i) soda evaporation at sintering temperatures, (ii) the development of duplex microstructures consisting of large grains (50 - 500 μm) in a fine-grained matrix and, (iii) conversion to β''-alumina often lags behind densification. The result of these constraints has been the development of rapid sintering processes at high temperatures (~ 1875 K) followed in some cases by annealing at lower temperatures to improve conversion to β''-alumina without coarsening the microstructure. Soda evaporation has been controlled by encapsulation in platinum [26], in β-alumina [11] and in magnesia [32]. A technique of zone sintering has also been used in which tubes are fed through a high temperature hot zone [33, 34] to provide a short, buffered firing cycle to minimize soda loss. At high temperatures densification proceeds more rapidly than grain growth and fine-grained materials with 97 - 99% theoretical density can be produced but the time at temperature needs to be kept short (5 - 40 min) to prevent exaggerated grain growth. Conversion to β''-alumina usually lags behind densification and so heat treatment at temperatures between 1625 and 1775 K is used to improve the ionic conductivity by increasing the volume

fraction of β''-alumina. The heat treatment temperature is chosen to avoid exaggerated grain growth although some matrix grain growth occurs and any residual stresses resulting from rapid cooling after sintering tend to be annealed out. A technique has been developed recently to produce high volume fractions of β''-alumina without annealing in which the powder is seeded with a small quantity (5 - 10%) of finely ground sintered β''-alumina. The seeding addition promotes full conversion to β''-alumina as this phase grows preferentially from the seeding agent. The grain size is determined by the number of nucleating centres and is typically in the range 25 - 75 μm [23].

An alternative to high temperature sintering processes is the use of very reactive powders or transient liquid phases to reduce the temperature to a level where soda loss and exaggerated grain growth no longer pose serious problems. A number of low melting point eutectic compositions exist in the Na_2O/Al_2O_3, $Na_2O/Li_2O/Al_2O_3$ and $Na_2O/MgO/Al_2O_3$ systems and have been used to enhance the sintering characteristics of beta-alumina [23, 35].

Ceramic properties

Microstructure and phase composition

The mechanical and electrical properties of beta-alumina are closely related to its microstructure and phase composition. The microstructure of beta-alumina generally consists of a fine-grained matrix with grains in the size range 0.5 - 2.0 μm for very rapidly sintered materials (Fig. 7) but rather coarser and with a somewhat larger size range for materials sintered at a lower rate (Fig. 8). Most beta-alumina ceramics have a duplex morphology to a greater or lesser degree with coarse grains in the fine-grained matrix as shown in Fig. 9; these are deleterious to the mechanical strength of the material as the conduction plane is also an easy cleavage plane. Seeding

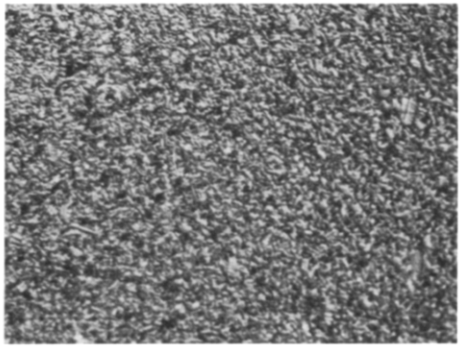

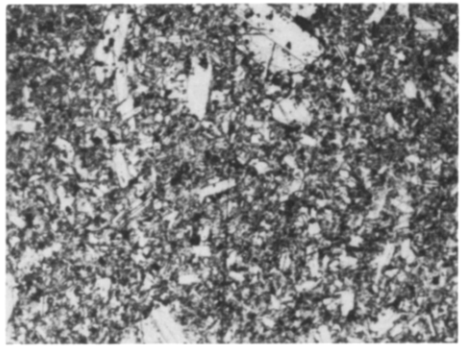

Fig. 7. Microstructure of beta-alumina rapidly sintered to produce a material with a grain size substantially all less than 2 μm, × 1000.

Fig. 8. Microstructure of beta-alumina sintered at a lower rate than that shown in Fig. 7. The grain size is larger in a range 2 - 10 μm with a few grains up to 30 μm, × 300.

Fig. 9. Microstructure of beta-alumina with a duplex morphology of coarse grains (~ 100 μm) in a fine-grained matrix, × 80.

Fig. 10. Microstructure of beta-alumina with a controlled, larger grain size in the range 20 - 60 μm produced by seeding with β''-alumina, × 200.

(a) (b)

Fig. 11. Transmission electron micrographs of fine grained matrix of beta-alumina showing grain size distribution and substructure with ceramic grains, (a) × 30 K, (b) × 100 K.

produces more equi-axed microstructures with grains in the size range 15 - 75 μm (Fig. 10). The phase composition is related to the chemical composition, sintering conditions and heat-treatment. In general increasing the level of doping with magnesia and lithia and increasing the soda content produces a corresponding increase in the volume fraction of β''-alumina [10, 36 - 38].

Examination of beta-alumina by transmission electron microscopy shows sharply faceted grains with a considerable amount of substructure within the ceramic grains (Fig. 11). Lattice imaging techniques have been successfully applied to beta-alumina and spacings corresponding to β- and β''- (00.1) type images have been observed [39 - 41]. Interpretation of these images is complicated by changes in the fringe spacing during electron irradiation. This has been interpreted as the movement of dislocations through the lattice [39] but a more detailed study [42] has shown that in β''-

alumina Na_2O evaporation results in the formation of spinel intergrowths by collapse of the Al–O–Al bridges and a simple shear displacement. The measured defect width is in agreement with the formation of this type of structure rather than mixed intergrowths of β- and β''-alumina [40]. More clearly defined dislocation networks and partial dislocations have been used to estimate the stacking fault energy of beta-alumina but transformation of β into β'' by a shear mechanism can be shown to require rearrangement in the spinel blocks and so only the defect structures described can be readily produced. β and β'' appear to exist as discrete units within a single grain with a width as small as 20 nm. Transformation from β to β'' clearly occurs by a reconstructive transformation in a nucleation and growth process. Other features such as intergranular phases [43], low-angle grain boundaries [44] and anti-phase boundaries [45] have also been seen in some materials. Little work has been carried out on the structure of grain boundaries and although they appear to be narrow and free from second phases [43], this is an area where there is considerable scope for further work.

The crystal structure of beta-alumina is substantially disordered. There are three possible sites for sodium in the sodium–oxygen layers of β-alumina consistent with the space group $P6_3/mmc$, 2*d*, 2*c* and 6*h* and early work showed that sodium occupied the 2*d* site [4]. These positions are referred to as BR (Beevers–Ross), aBR (anti-Beevers–Ross), and mO (mid-oxygen) sites, respectively. Later and more refined structural work [46] showed that the sodium did not simply occupy BR sites but was distributed in a triangular pattern with three quarters of the sodium density close to the BR and the remainder in the mO position. The aBR position was empty. This disorder accounts for the rapid diffusion in the basal plane as sodium ions can readily exchange positions between occupied and vacant sites. There is an excess of sodium ions in β-alumina and charge compensating defects are required to preserve electrical neutrality. These may be Al^{3+} vacancies or O^{2-} interstitials but in fact neutron diffraction studies [47] have identified a compound defect that has the formula:

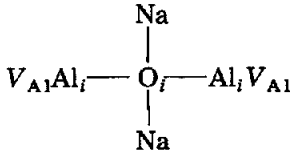

where $V_{Al}Al_i$ is a Frenkel defect (an aluminium vacancy–oxygen interstitial pair) and O_i is an interstitial oxygen ion in the mO position in the conduction plane. This defect is not observed in β''-alumina and the spinel blocks are essentially free of vacancies and interstitial aluminium ions.

Ionic conductivity

The overall resistivity r_t of a polycrystalline beta-alumina membrane is the sum of the grain bulk resistivity r_b which is equivalent to the single

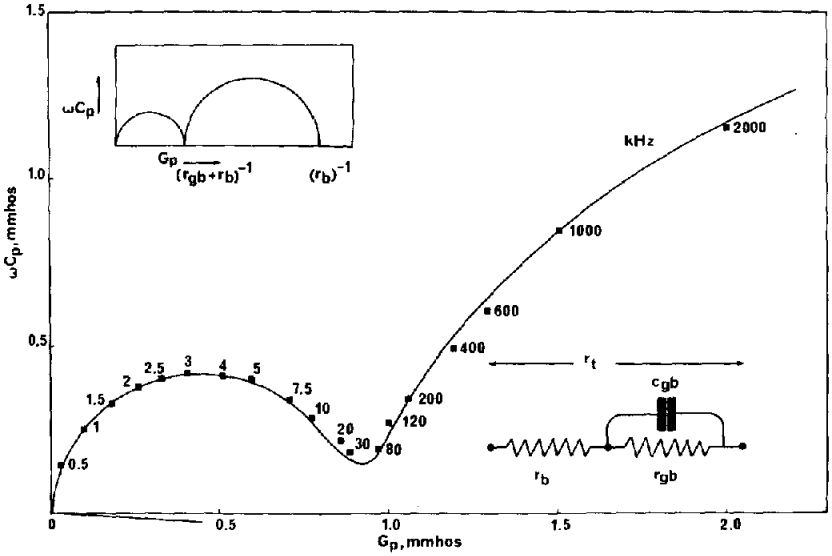

Fig. 12. Complex plane plot of the real, G_p, and imaginary, ωC_p, parts of the admittance for beta-alumina with a grain size of 35 μm and a volume fraction of β'' of 0.9 (Fig. 10) measured at 294 K over the range of frequencies shown. The insets show the form of equivalent circuit assumed and the ideal form of the complex plane plot for this circuit. The intersection of the low frequency semi-circle with the real axis gives the total resistivity and the intersection of the high frequency semi-circle with the same axis, the grain bulk (single crystal) resistivity.

crystal value and the grain boundary resistivity r_{gb} with an associated grain boundary capacitance C_{gb}. Four-terminal d.c. measurements give values of the overall resistivity but a.c. measurements allow the components of the equivalent circuit to be separated by complex plane plotting. For example, the real, G_p, and imaginary parts, ωC_p, of the admittance have an idealized complex admittance plot as shown in Fig. 12 in the form of two semi-circles that intersect with the real axis to give the overall resistivity and the bulk resistivity at sufficiently high frequency. There are experimental problems with this technique in that very high frequencies (> 5 MHz) are often necessary to resolve a substantial part of the high frequency semi-circle. The ionic conductivity σ follows an Arrhenius relation of the form:

$$\sigma = (\sigma_0/T) \exp\{-(E_a/RT)\}$$

where σ_0 is a constant, T is the absolute temperature, E_a the activation energy for ionic motion and R the gas constant. Values for the ionic resistivity of single crystal samples of undoped β-alumina and magnesium-doped β''-alumina [1, 48, 49] have been determined as ~ 0.05 Ωm at 575 K respectively with activation energy in both cases of ~ 13 kJ/mol. The ionic resistivity of polycrystalline materials is typically 0.12 Ωm for β-alumina and 0.03 Ωm for β''-alumina at 575 K (Fig. 13, Table 1). The increase over single crystal values is partly caused by grain boundary contributions and partly by

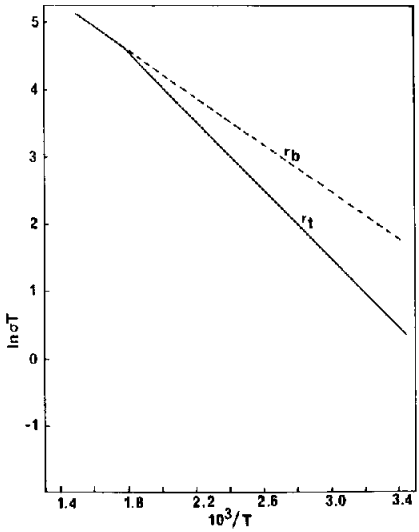

Fig. 13. Arrhenius plot of ln σT (σ, ionic conductivity; T, absolute temperature) against reciprocal temperature showing the overall resistivity r_t and the grain bulk resistivity r_b separately. The beta-alumina sample is similar to that shown in Fig. 10.

TABLE 1

Electrical properties of beta-alumina

Ionic resistivity (σ)	
β-alumina (single crystal)	0.05 Ωm (575 K)
activation energy (E_a)	13 kJ/mol
β-alumina (polycrystalline)	0.12 Ωm (575 K)
activation energy (E_a)	24 kJ/mol
β''-alumina (single crystal)	0.01 Ωm (575 K)
activation energy (E_a)	13 kJ/mol
β''-alumina (polycrystalline)	0.05 Ωm (575 K)
activation energy (E_a)	20 kJ/mol
Electronic resistivity [64]	$\sim 0.5 \times 10^9$ Ωm (575 K)
(Wagner technique measurements)	$> 1.0 \times 10^9$ Ωm (300 K)

the tortuous path ions have to follow in a polycrystalline material. The overall activation energy of polycrystalline materials tends to be higher than single crystal values because the activation energy associated with the grain boundaries is rather higher than the grain bulk but the contribution this makes to the overall activation energy is dependent on the grain boundary area per unit volume and to a lesser extent temperature. The activation energy for conduction in the grain bulk measured by a.c. techniques is virtually the same as that measured in single crystals.

There is, then, a close relationship between the microstructure and phase composition of beta-alumina and for high conductivity the volume fraction of β''-alumina needs to be maximized and the grain boundary component of the overall resistivity minimized.

Mechanical properties

The strength, σ_f, of beta-alumina, in common with other ceramic materials, is largely governed by the stress necessary to propagate small microstructural flaws according to a modified Griffith relationship:

$$\sigma_f = 1.25\sqrt{E\gamma_i/c}$$

where γ_i is the fracture initiation energy, c is radius of the flaw and E is Young's modulus. Flaws may take the form of inclusions, voids, surface or interior cracks or excessively large grains. Measurement of the fracture strength as a function of defect size or crack length allows estimates of the fracture energy to be made (Fig. 14). Values are typically ~ 15 J/m^2 [50 - 52] and the corresponding values for the critical stress intensity factor $K_{Ic} = \sqrt{2E\gamma_i}$ are ~ 2.7 $MN/m^{3/2}$ with a Young's modulus of 2.1×10^{11} N/m^2 (see Table 2). Strength values of 230 - 280 MN/m^2 are typical for sintered fine-grained material (< 5 μm); seeded material with a grain size of ~ 35 μm has a strength in the range 150 - 180 MN/m^2 but completely coarse grained material which had been allowed to undergo abnormal grain growth to a size 150 - 250 μm has strengths of ~ 20 MN/m^2. The tensile strength of a group of beta-alumina rings with a fine-grained microstructure tested in diametral compression is shown in Fig. 15. Higher strengths have been measured for

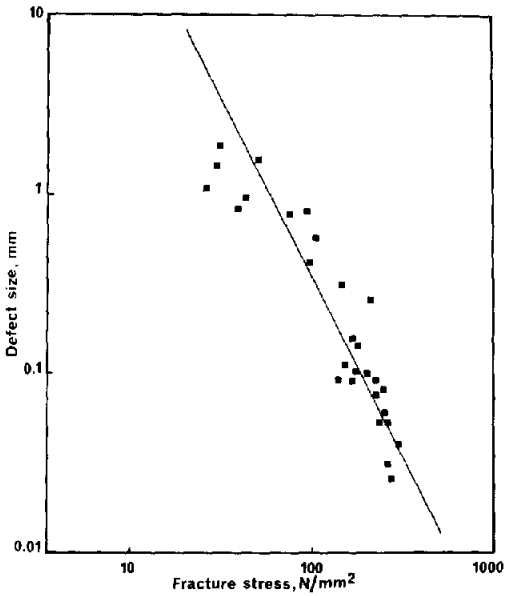

Fig. 14. Fracture strength of beta-alumina samples as a function of defect size.

TABLE 2

Mechanical properties of beta-alumina

Tensile strength (σ_f) (grain size < 5 μm, equiaxed)	230 - 250 MN/m^2 (98% theoretical density)
	310 - 330 MN/m^2 (hot-pressed)
Critical fracture energy (γ)	13 J/m^2
Critical stress intensity factor (K_{Ic})	2.7 MN/m$^{3/2}$
Hardness	1400 VPN
Young's modulus (E)	2.1 x 10^{11} N/m^2
Bulk modulus (K)	1.5 x 10^{11} N/m^2
Poisson's ratio (μ)	0.27

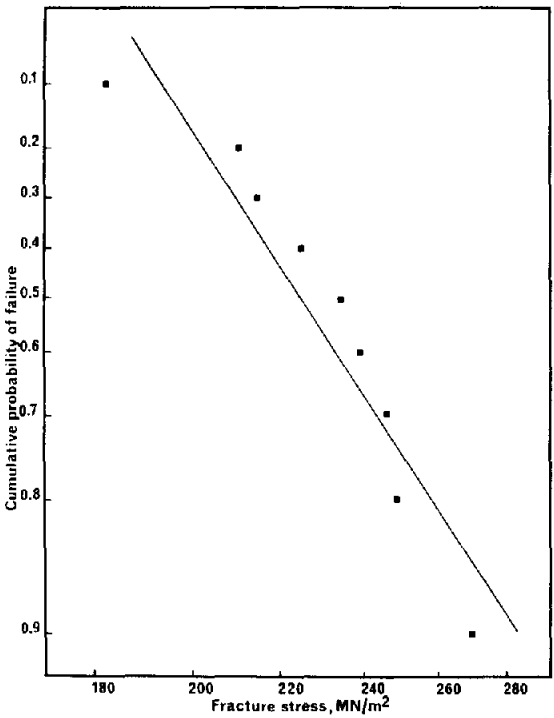

Fig. 15. Cumulative probability of tensile failure of small rings of fine grained beta-alumina.

hot-pressed materials. There is evidence that weaker materials are less durable in cells but it would appear that above a threshold level of ~ 150 MN/m^2 cell lifetime becomes less sensitive to mechanical strength.

Some of the defects observed in beta-alumina have been characterized by direct observation. The majority take the form of small pores with

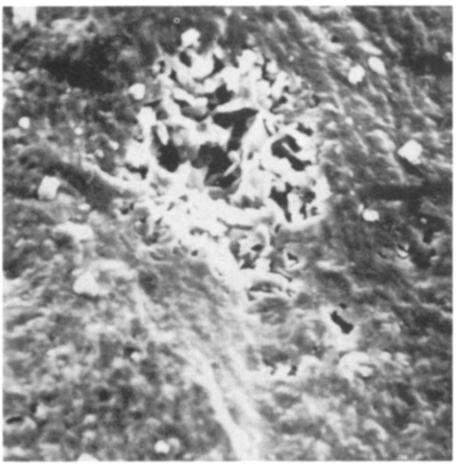

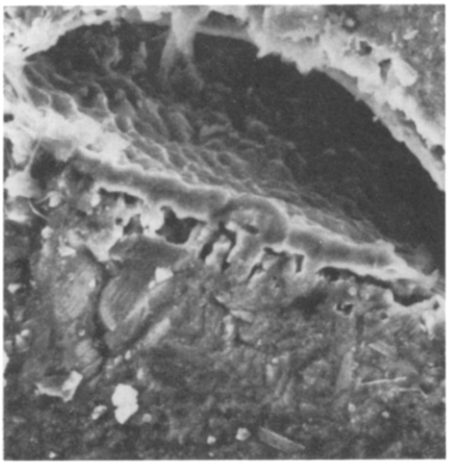

Fig. 16. Defect containing small beta-alumina crystallites on fracture surface, (× 280).

Fig. 17. Coloured defect with Ni and Fe impurities and solidified, glassy material on the inner surface of the defect, (× 640).

various associated impurities although some small cracks are present. The most numerous type of defect is areas of high porosity containing well developed crystallites of beta-alumina (Fig. 16). These are either discrete pores or localized groups of smaller pores. They show slightly higher Na contents and are evidently the result of local inhomogeneities in the powder. Other defects are characteristically blue, black or brown in colour and have Co, Ni and Fe impurities probably as a result of metallic impurities in the powder. A typical defect is shown in Fig. 17. It is doubly important to eliminate defects from beta-alumina, not only because they weaken the ceramic, but also because they may contribute to the failure of the solid electrolyte during cell operation by causing inhomogeneous ionic transport.

Thermal and other properties

Several other properties of beta-alumina are important for operation in electrochemical cells. In particular its thermal shock resistance so that it can withstand temperature excursions during manufacture or operation; its thermal expansion coefficient because of the necessity to join beta-alumina to other cell components; its thermal conductivity; and its wetting behaviour.

The thermal conductivity k of beta-alumina has been determined indirectly from measured values of the density ρ, the specific heat c and the thermal diffusivity D using the relationship [53]:

$$k = \rho c D$$

Density is typically 3230 kg/m^3 for sintered materials and the specific heat varies from ~ 950 J/kgK at 300 K to ~ 1100 J/kgK at 680 K. The thermal diffusivity has been measured by a temperature transient method and varies from 1.0 mm^2/s at 300 K to 0.8 mm^2/s at 680 K. Correspondingly the

TABLE 3

Thermal properties of beta-alumina

Thermal expansion coefficient	
β-alumina [54]	a-axis 7.7×10^{-6} K^{-1} (775 - 875 K)
	c-axis 5.7×10^{-6} K^{-1} (775 - 875 K)
β''-alumina [56]	a-axis 7.8×10^{-6} K^{-1} (675 - 1275 K)
	c-axis 7.3×10^{-6} K^{-1} (675 - 1275 K)
Polycrystalline material	7.2×10^{-6} K^{-1} (300 - 675 K)
Thermal diffusivity, D (polycrystalline material)	1.0 mm^2/s (300 K) 0.8 mm^2/s (680 K)
Specific heat, c (polycrystalline material)	950 Jkg/K (300 K) 1100 Jkg/K (680 K)
Thermal conductivity, k (polycrystalline material)	3.0 W/mK (300 K) 2.9 W/mK (680 K)

TABLE 4

Thermal shock resistance

	Material		
	β/β''-Al_2O_3	α-Al_2O_3	Fused SiO_2
Tensile strength, σ_f (MN/m^2)	240	400	100
Poisson's ratio, μ	0.27	0.28	0.17
Young's modulus, E, $\times 10^{11}$ (N/m^2)	2.1	3.8	0.7
Thermal expansion coefficient, α, $\times 10^{-6}$(K^{-1})	7.2	8.8	0.5
Thermal conductivity k (W/mK)	3.0	35	1.5
$R = \frac{\sigma_f(1-\mu)}{E_a} \times 10^{-2}$ K	11.6	8.6	237
$R^1 = Rk \times 10^{-2}$ W/m	34.8	301	356

thermal conductivity k varies only slightly from 3.0 W/mK at 300 K to 2.9 W/mK at 680 K. The thermal conductivity changes slightly with composition and microstructure and is low compared with α-alumina with a typical value of 35 W/mK. The thermal expansion coefficient of polycrystalline beta-alumina is 7.2×10^{-6} K^{-1} over the range from room temperature to 700 K. This is sufficiently close to α-alumina to allow beta-alumina components to be joined to α-alumina insulating components with relatively few problems. Mechanical and thermal property data (Tables 2 and 3) can be

combined to calculate a figure of merit, R, that gives a measure of the thermal shock resistance of the materials where:

$$R = \frac{\sigma_f(1-\mu)}{E\alpha}$$

This expression is only strictly valid for an infinitely fast quench and a further figure $R^1 = Rk$ can also be calculated to give a comparison between materials for a finite cooling rate. Values of R and R^1 for beta-alumina, α-alumina and fused silica, which has a very good thermal shock resistance, are shown in Table 4 and it is clear that with very rapid cooling rates the behaviour of beta-alumina and α-alumina should be similar but with more moderate cooling beta-alumina will tend to have a rather inferior performance. Experimental data for beta-alumina samples quenched rapidly into water show that it can withstand a temperature differential of ~ 160 K without loss of strength [23] whereas α-alumina with a similar microstructure could withstand 220 K (Fig. 18).

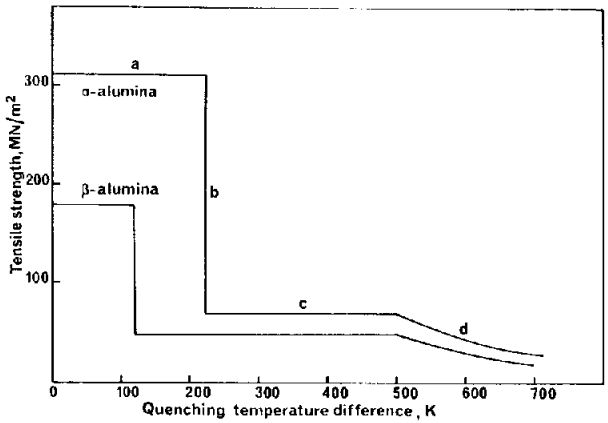

Fig. 18. Variation of tensile strength of α-alumina and β-alumina samples down quenched by the temperatures indicated. Both materials show a region (a) of constant strength with no fracture nucleation; (b) an instantaneous drop in strength due to crack propagation; (c) a region of constant strength where the cracks remain sub-critical and (d) a gradual decrease in strength as the cracks produced increase in size [23].

The wetting of beta-alumina by liquid sodium has been studied between 470 and 670 K by measurement of the contact angle of sodium on beta-alumina tubes. Wetting did not occur at temperatures below 570 K but at 620 K the electrolyte was wetted irreversibly [56]. The wetting behaviour was correlated with the behaviour of sodium/beta-alumina/sodium cells in that at temperatures where wetting had occurred, the contact resistance was minimal and the resistance of the cell was that calculated using the bulk resistance of the electrolyte determined separately by a 4-terminal d.c. technique.

Time dependent properties

Attempts have been made to correlate the failure of beta-alumina electrolyte with the quantity of sodium passed through the membrane. Failure is associated with the formation or penetration of sodium in the electrolyte. This may be present either as grey filaments or as a general darkening extending from the sodium/beta-alumina interface. A number of methods have been used to detect sodium penetration into the bulk of the material; for instance, Auger electron spectroscopy [57] has been used to show that the concentration of sodium on the fracture surface of material operated in sodium–sulphur cells was greater than on unused material. Filaments of sodium have been observed directly by exposing beta-alumina to chlorine and observing the sodium chloride filaments formed [58] and indirectly by following the impedance of a sodium/beta-alumina/sodium cell passing constant current at 675 K [59]. This showed that the sodium filaments grew as dendrites and breakdown of the electrolyte occurred when the material became an electronic conductor with metallic sodium dendrites extending through the material. Cracking has also been detected directly by acoustic emission during electrolysis in sodium/beta-alumina/sodium cells [60].

Phenomenologically, damage appears to occur when sodium ions efflux from a crack and two models have been put forward to account for this deterioration process. In one model [59], surface cracks become filled with liquid sodium and extend because the Poiseuille pressure resulting from the flow of metal in the crack exceeds the fracture stress of the material at the crack tip. There will be a spectrum of crack growth rates depending on the initial defect size but in general crack propagation will be proportional to the current density. The flow of sodium in the crack is enhanced by current focusing which occurs because a crack filled with sodium on the egress side of the membrane will act as a current concentrator since the conductivity of metallic sodium is $\sim 10^6$ greater than beta-alumina. The sodium filled crack thus provides a lower resistance path than the surrounding beta-alumina and with a potential gradient across the membrane, sodium ions will focus at the crack tip. An alternative model [61] provides an explanation for some other observations, in particular a threshold current density below which dendritic penetration is not apparent. This model makes the assumption that sodium wets the ceramic and that it is soluble to a very small degree in liquid sodium. The chemical potential of a crack tip with a sharp radius will be lower than the rest of the crack because of its negative curvature and in consequence material will tend to dissolve on the crack faces under the driving force of capillarity and redeposit at the tip, blunting the crack. But under conditions of electrolysis, the enhanced flow of sodium through the crack tip will carry away solute because the sodium close to the crack tip is unsaturated with beta-alumina and continuously replenished. The Poiseuille pressure produced by sodium flowing in the crack causes mechanical stress which increases the chemical potential of the crack tip. The crack blunting

due to capillarity must, then, be exceeded by the effects of mass transport of sodium through the electrolyte and this provides an explanation for the threshold current density for degradation. The model also shows that delayed fracture may occur on static loading in liquid sodium and this has been examined experimentally.

Under static loading, the rate of crack growth V is related to the stress intensity factor K_I ($= \sqrt{2E\gamma_i}$) as:

$$V = aK_I^n$$

where a is a constant and the power n denotes an empirical relationship between crack velocity and stress intensity factor. Accordingly there is a strain rate dependence of strength such that the ratio of strengths $\sigma_{1,2}$, at two strain rates $\dot{\epsilon}_{1,2}$, is given by:

$$(\sigma_1/\sigma_2)^{n+1} = \dot{\epsilon}_1/\dot{\epsilon}_2$$

Carrying out mechanical tests over a wide range of strain rates in liquid sodium at 575 K and in air at room temperature has shown that for beta-alumina n is > 100 which is in the range observed for non-oxide ceramics such as silicon carbide or silicon nitride whereas for oxides n is typically 10 - 30. In view of the apparently high value more precise values are obtained by carrying out dead-load tests to effectively extend the range of strain rates. Under conditions of constant applied stress, the ratio of failure times $t_{1,2}$ under applied stresses $\sigma_{1,2}$ is given by:

$$(\sigma_1/\sigma_2)^n = t_2/t_1$$

Data are interpolated to correspond to a fixed time and a value of n is determined that provides the best agreement. The failure stress of beta-alumina tested under delayed fracture conditions in liquid sodium at 575 K has shown that it is > 150 [62]. Beta-alumina shows an abnormally low time dependence of strength under stress both in ambient conditions and in liquid sodium at cell temperatures. There is clearly a considerable amount of work that needs to be done to characterize the failure mechanisms of beta-alumina under conditions of electrolysis.

Ion exchange with impurities in the electrodes and the build-up of surface contaminants will also have an effect on the life of the electrolyte and on its conductivity. An increase in resistivity of beta-alumina resulting from potassium contamination has been noted in cells with glass containers [63] but potassium is a contaminant in most grades of sodium and the permissible levels for this and other impurities will need to be determined experimentally.

Conclusions

The development of beta-alumina electrolytes for power sources, in particular for the sodium–sulphur battery, has reached a critical stage in many laboratories. The material properties for optimum cell performance

and durability have been established and although there is considerable scope for further improvements, several programmes are moving from a phase of scientific research to engineering development. All manufacturing routes involve the sintering of a consolidated powder in the solid state and the choice of the green forming stage places constraints on the method of powder production. The principal requirement in sintering of beta-alumina is the need to control the atmosphere in the furnace to minimize loss of sodium oxide from the ceramic and several methods of achieving this have been devised.

The properties of beta-alumina that are of principal importance for application in power sources are its ionic conductivity and mechanical strength. Conversion of the material to the more conductive β'' phase improves the overall ionic conductivity but extended firing or annealing times are necessary to produce full conversion and these tend to reduce the mechanical strength of the material by inducing the growth of large ceramic grains in an otherwise fine-grained material. Typically, ionic resistivities are in the range 0.04 - 0.12 Ωm at 575 K and mechanical strengths > 200 MN/m^2. Dopants, usually magnesium and lithium, are used to stabilize the β'' phase. The thermal properties of beta-alumina are also important as they determine limits to various operating parameters and define some of the materials requirements for other device components. The thermal expansion coefficient of beta-alumina is such that it can be readily joined by means of appropriate glasses to α-alumina components for the manufacture of electrically insulating seals. The thermal shock resistance is relatively poor, largely because of the low thermal conductivity of beta-alumina, but adequate for most purposes, especially in thin sections which are preferred for cell operation. Beta-alumina is not readily wetted by liquid sodium at temperatures below 620 K but is irreversibly wetted at temperatures above this limit.

Failure of beta-alumina during cell operation is associated with a general darkening of the ceramic or with the formation of dendrites of sodium extending through the ceramic which eventually cause breakdown when they produce electronic conduction through the electrolyte. Stress corrosion cracking of beta-alumina in liquid sodium at 575 K in the absence of current flow does not, however, appear to be a problem as crack growth rates are considerably lower than for comparable ceramic materials. The characterization of failure mechanisms of beta-alumina under conditions of electrolysis remains an area where a considerable amount of work remains to be done although materials with satisfactory lifetimes have been identified.

The material properties of beta-alumina set a limit to the impedance of the electrolyte per unit area. For a material with an ionic resistivity of 0.06 Ωm at 575 K and a membrane thickness of 1.5 mm, the impedance is 90 Ωmm^2. Small improvements in the conductivity and decreases in the membrane thickness can reduce this but larger reductions can be made by changing the cell configuration. Consequently cell designs with larger areas of electrolyte and electrodes for the same volume of active material are being developed to optimize power density requirements although this tends to be

achieved at the expense of energy density. In these designs, increasing the electrode/electrolyte area allows the distance that sodium ions have to travel both through the membrane and in the cathode to be minimized whilst the flow of electrons takes place in a plane normal to the electrodes. In simple terms, long, thin electrolyte tubes give higher power densities than shorter, larger diameter tubes with the same quantity of active materials.

It seems likely, then, that beta-alumina electrolyte materials will be developed to the point where they are used commercially in a wide variety of devices. Measuring devices apart, the first of these will almost certainly be the sodium–sulphur battery but the range of potential applications for sodium–beta-alumina and for substituted beta-aluminas is growing very rapidly.

Acknowledgement

The permission of Chloride Silent Power Limited to publish this paper is gratefully acknowledged.

References

1 J. T. Kummer, Prog. Solid State Chem., 7 (1972) 141.
2 P. W. McGeehin and A. Hooper, J. Mater. Sci., 12 (1977) 1.
3 W. L. Bragg, C. Gottfried and J. West, Z. Kristallogr., 77 (1931) 255.
4 C. A. Beevers and M. A. Ross, Z. Kristallogr., 97 (1937) 59.
5 Y. Yamaguchi and K. Suzuki, Bull. Chem. Soc. Japan, 41 (1968) 93.
6 M. Bettman and C. R. Peters, J. Phys. Chem., 73 (1969) 1774.
7 N. Weber and J. T. Kummer, Adv. Energy Conv. Eng. A.S.M.E. Conf. Florida, (1976) p. 913.
8 G. J. May and I. W. Jones, Metall. Mater. Technol., 8 (1976) 427.
9 S. Hattori, M. Yamaura, S. Kimura and S. Iwabuchi, S.A.E. Paper 770281 (1977).
10 R. Bauer, W. Haar, H. Kleinschmager, G. Weddigen and W. Fischer, J. Power Sources, 1 (1976/77) 109.
11 J. Fally, C. Lasne, Y. Lazennec and P. Margotin, J. Electrochem. Soc., 120 (1973) 1296.
12 S. P. Mitoff and J. B. Bush, Proc. 9th Intersoc. Energy Conv. Eng. Conf., 1975, p. 916.
13 J. Werth, I. Klein and R. Wylie, Energy Storage, The Electrochemical Society, Princeton, New Jersey, 1976, p. 198.
14 F. G. Will and S. P. Mitoff, J. Electrochem. Soc., 122 (1975) 457.
15 K. O. Hever, J. Electrochem. Soc., 115 (1968) 830.
16 G. J. Dudley, B. C. H. Steele and A. T. Howe, J. Solid State Chem., 18 (1976) 141.
17 N. Weber, Energy Conversion, 14 (1974) 1.
18 Y. Ito, S. Yoshizawa and S. Nakamatsu, J. Appl. Electrochem., 6 (1976) 361.
19 D. J. Fray, Metall. Trans., 8B (1977) 153.
20 W. Baukal, H. P. Beck, W. Kuhn and R. Siegler, in D. H. Collins (ed.), Power Sources 6, 1976, Academic Press, London, 1977, p. 655.
21 L. N. Glyzina, V. I. Faddeva and Y. D. Tretyakov, Inorg. Mat., 11 (1975) 927.
22 S. E. Weiner, Research on electrodes and electrolyte for the Ford sodium–sulphur battery, Report on Contract No. NSF-C805 (AER-73-07199) July 1975.

23 S. E. Weiner, Research on electrodes and electrolyte for the Ford sodium–sulphur battery, Report on Contract No. NSF-C805 (AER-73-07199) January 1976.
24 S. E. Weiner, Research on electrodes and electrolyte for the Ford sodium–sulphur battery, Report on Contract No. NSF-C805 (AER-73-07199) January 1977.
25 M. P. Pechini, U.S. Pat. 3,330,697.
26 G. E. Youngblood, A. V. Virkar, W. R. Cannon and R. S. Gordon, Ceram. Bull., 56 (1977) 206.
27 P. Popper, Isostatic Pressing, Heyden, London, 1976.
28 J. M. Andrews, A. H. Collins, D. C. Cornish and J. Dracass, Proc. Br. Ceram. Soc., 12 (1969) 211.
29 R. W. Powers, J. Electrochem. Soc., 122 (1975) 490.
30 J. H. Kennedy and A. Foissy, J. Electrochem. Soc., 122 (1975) 482.
31 W. Byckalo, G. Rosenblatt, J. Lam and P. S. Nicholson, Ceram. Bull., 55 (1976) 286.
32 J. L. Sudworth, Proc. 10th Intersoc. Energy Conv. Eng. Conf., New York, 1975, p. 624.
33 I. W. Jones and L. J. Miles, Proc. Br. Ceram. Soc., 19 (1971) 161.
34 D. Chatterji, Development of sodium–sulphur batteries for utility application, EPRI EM-266, Report No. 128-3, December 1976.
35 L. C. DeJonghe and H. Chandan, Ceram. Bull., 55 (1976) 312.
36 L. J. Miles and I. W. Jones, Proc. Br. Ceram. Soc., 19 (1969) 179.
37 J. H. Kennedy and A. F. Sammells, J. Electrochem. Soc., 119 (1972) 1609.
38 M. D. Hames and J. H. Duncan, S.A.E. Paper 750375 (1975).
39 L. C. DeJonghe, Mat. Res. Bull., 12 (1977) 627.
40 D. J. M. Devan, B. Hudson and P. T. Moseley, Mater. Res. Bull., 9 (1974) 1073.
41 R. Stevens and L. J. Miles, J. Mater. Sci., 11 (1976) 1911.
42 R. Stevens, J. Mater. Sci., 9 (1974) 801.
43 L. C. DeJonghe, personal communication.
44 L. C. DeJonghe and M. Y. Hsieh, Proc. Symp. and Workshop on Advanced Battery Research March 22 - 24 1976, Argonne National Laboratory B13, ANL Rep. 76-8.
45 Y. LeCars, D. Gratias, R. Portier and J. Thery, J. Solid State Chem., 15 (1975) 218.
46 C. R. Peters, M. Bettman, J. W. Moore and M. P. Glick, Acta Crystallogr., B27 (1971) 1826.
47 W. L. Roth, F. Reidinger and S. LaPlaca, in G. D. Mahon and W. L. Roth (eds.), Superionic Conductors, Plenum, New York, 1976, p. 223.
48 W. L. Fielder, H. E. Kautz, J. S. Fordyce and J. Singer, J. Electrochem. Soc., 122 (1975) 528.
49 R. D. Armstrong, T. Dickinson and P. M. Willis, J. Electroanal. Chem., 67 (1976) 121.
50 S. R. Tan and G. J. May, J. Mater. Sci., 12 (1977) 1058.
51 R. Stevens, J. Mater. Sci., 9 (1974) 934.
52 A. V. Virkar and R. S. Gordon, J. Am. Ceram. Soc., 60 (1977) 58.
53 S. N. Ruddlesden, personal communication.
54 R. Ridgway, A. Klein and W. O'Leary, Trans. Electrochem. Soc., 70 (1936) 71.
55 R. H. Radzilowski, J. Am. Ceram. Soc., 53 (1970) 699.
56 A. Gibson, in D. H. Collins (ed.), Power Sources 6, Academic Press, London, 1977, p. 673.
57 C. T. H. Stoddart and E. D. Hondros, Trans. Br. Ceram. Soc., 73 (1974) 61.
58 J. L. Sudworth, M. D. Hames, M. A. Storey, M. F. Azim and A. R. Tilley, in D. H. Collins (ed.), Power Sources 4, Oriel Press, Newcastle upon Tyne, 1972.
59 R. D. Armstrong, T. Dickinson and J. Turner, Electrochim. Acta, 19 (1974) 187.
60 C. A. Worrell, personal communication.
61 R. H. Richman and G. J. Tennenhouse, J. Am. Ceram. Soc., 58 (1975) 63.
62 R. W. Davidge, J. McLaren, G. Tappin and G. J. May, unpublished research.
63 Y. Lazennec, C. Lasne, P. Margotin and J. Fally, J. Electrochem. Soc., 122 (1975) 734.
64 A. Hooper, personal communication.